

1 **Continuous Monitoring of a Soil Aquifer Treatment System’s Physico-Chemical**  
2 **Conditions to Optimize Operational Performance**

3

4 Tuvia Turkeltaub<sup>1</sup>, Alex Furman<sup>2</sup>, Ron Mannheim<sup>2</sup>, Noam Weisbrod<sup>1</sup>

5 <sup>1</sup>Department of Environmental Hydrology and Microbiology, Zuckerberg Institute for Water  
6 Research, The Jacob Blaustein Institutes for Desert Research, Ben-Gurion University of the  
7 Negev, Sede Boqer Campus, Midreshet Ben-Gurion, 84990 Israel.

8 <sup>2</sup>Technion – Israel Institute of Technology, Civil and Environmental Engineering, Haifa 32000,  
9 Israel

10

11 *Correspondence to: Tuvia Turkeltaub (tuvat@bgu.ac.il)*

12

13 **Highlights**

- 14 • *Long wetting stages reduce soil percolation capabilities during winter.*  
15 • *Redox and gaseous O<sub>2</sub> display intensive dynamics in the top 25 cm of the soil aquifer*  
16 *treatment vadose zone.*  
17 • *Optimal wetting and drying stages are defined according to E<sub>h</sub> and gaseous O<sub>2</sub>*  
18 *observations.*  
19 • *The length of wetting and drying stages should be defined separately rather than by*  
20 *adhering to their ratio.*

21

22

23

24 **Abstract**

25 Soil aquifer treatment (SAT) is a tertiary process for wastewater treatment where the wastewater  
26 infiltrates through a thick vadose zone for purification and storage in the underneath aquifer.  
27 SAT infiltration basins are typically flooded intermittently, while maintaining a fixed ratio  
28 between the wetting and the drying stages. However, infiltration basins exhibit different physical  
29 and chemical properties, limiting the generalization of SAT operation to attain optimal  
30 efficiency. Since frequent sampling of the soil pore water to verify the SAT's biodegradation  
31 efficiency can be arduous, continuous monitoring of the SAT vadose zone's physico-chemical  
32 conditions is required. In this study, redox potential ( $E_h$ ) was continuously monitored, together  
33 with other variables such as volumetric water content ( $\theta$ ), soil temperature, and gaseous oxygen  
34 ( $O_2$ ), at multiple depths of a SAT vadose zone throughout the year and while the system was  
35 constrained to different operational modes. Hydrological models were calibrated and validated to  
36 water content observations, and they illustrated the seasonal changes in water infiltration.  
37 Furthermore, it was shown that under long wetting stages during winter, there was a reduction in  
38 the SAT's drainage capabilities. The  $E_h$  observations, under long wetting stages, demonstrated  
39 larger variability and very negative values as ambient temperature increased. Assembling the  
40 daily  $E_h$  observations illustrated that a wetting stage should cease after about 30 hours, once  
41 suboxic conditions are established. A drying stage's optimal duration should be 36 hours,  
42 according to the  $E_h$  and  $O_2$  observations during summer and winter. Ultimately, the study shows  
43 that the length of wetting and drying stages should be defined separately, rather than by adhering  
44 to the wetting/drying ratio.

45

46

## 47 **1 Introduction**

48 Worldwide water scarcity has motivated the development of alternative water resources such as  
49 the reuse of treated wastewater. Soil aquifer treatment (SAT) is commonly implemented to  
50 further improve the recovered water's quality and remove the majority of suspended matter,  
51 microorganisms, viruses, and organic and inorganic constituents (Dillon, 2005; Goren et al.,  
52 2014; Massmann et al., 2006; Schmidt et al., 2011; Tsangaratos et al., 2017). In SAT systems,  
53 the treated wastewater is recharged to the underlying aquifer by surface spreading over  
54 infiltration basins. The wastewater is purified mainly through the physical and biochemical  
55 processes that occur during water passage through the vadose zone (Dillon, 2005; Elkayam et al.,  
56 2015). Although SAT systems have been used for decades (Grinshpan et al., 2021; Bouwer,  
57 2002), the ability to estimate and predict a SAT system's performance is still challenging, and  
58 the optimal SAT operation is still under investigation (Ben Moshe et al., 2020; Sharma and  
59 Kennedy, 2017).

60 A major uncertainty in SAT systems concerns the vadose zone processes that play a central role  
61 in determining the quality of the water that recharges the aquifer (Elkayam et al., 2015). The  
62 chemistry of the percolating wastewater changes due to a combination of several biogeochemical  
63 processes, such as organic matter biodegradation, nitrification, sorption, cation exchange, etc.  
64 (Amy and Drewes, 2007; Díaz-Cruz and Barceló, 2008; Goren et al., 2014; Miller et al., 2006;  
65 Tufenkji et al., 2003). Most of the organic matter is removed by biodegradation (i.e. microbial  
66 activity) within the upper two meters of the vadose zone (Drewes, 2009). Nevertheless, the  
67 microbial activity is greatly affected by the soil water content, which frequently changes in SAT.  
68 Generally, a major challenge in SAT systems is to facilitate the intrusion of O<sub>2</sub>, primarily in the  
69 gaseous phase, and to enrich the active subsurface with O<sub>2</sub> (Ben Moshe et al., 2020; Massmann  
70 et al., 2006).

71 A consequence of the perturbation in the O<sub>2</sub> supply to SAT is expressed in changes in the redox  
72 conditions (Mächler et al., 2013; Rezanezhad et al., 2014). Redox potential or oxidation-  
73 reduction potential is a quantitative measure of electron availability, i.e., the tendency of the  
74 system to receive or donate electrons (Hinchey and Schaffner, 2005). Substantial changes in  
75 SAT systems' redox conditions might lead to the release of undesirable metals, such Fe<sup>2+</sup> and

76  $Mn^{2+}$  (Goren et al., 2012), and affect the degradation rates of pesticides and pharmaceutical  
77 substances (Massmann et al., 2006). Additionally, previous studies have illustrated the possible  
78 degradation of groundwater quality due to the emergence of contaminants that leach from the  
79 SAT vadose zone under reducing conditions (Asano and Cotruvo, 2004; Massmann et al., 2006;  
80 Oren et al., 2007; Sharma and Kennedy, 2017). Redox processes are associated with the  
81 degradation of organic matter by terminal electron acceptors or redox couples, such as  $O_2/H_2O$ ,  
82  $NO_3/N_2$ ,  $MnO_2/Mn^{2+}$ ,  $Fe^{3+}/Fe^{2+}$ , and  $SO_4/H_2S$ , in sequential order from the highest energy yield  
83 downwards (Berner, 1981; Froelich et al., 1979; Christensen et al., 2000). The transition between  
84 redox conditions is determined by the presence and availability of these electron  
85 acceptors/donors. Once the strongest oxidizing species ( $O_2$ ) is depleted, the next strongest  
86 oxidizing species is used ( $NO_3$ ) and so on. The alternation between oxic ( $> 400$  mV), suboxic  
87 (between 400 and -100 mV), and anoxic (-100 mV  $>$ ) conditions in the vadose zone depends on  
88 the availability of the oxidized species (Reedy et al., 2000). In addition, studies have reported on  
89 the seasonal (temperature changes) effects on redox conditions, which were attributed to the  
90 increase in dissolved oxygen concentrations at low temperatures (Massmann et al., 2006) and the  
91 greater microbial activity (i.e., higher  $O_2$  consumption) at higher temperatures (Greskowiak et al.,  
92 2006; Kirschbaum, 1995).

93 An important operational aspect of a SAT system is the intermittent application of the effluents  
94 (Sattar, 2016; Sallwey et al., 2020). After the infiltration basin is flooded with wastewater, a  
95 drying period is implemented to sustain the SAT's infiltration capacity and biochemical  
96 capabilities (Sharma and Kennedy, 2017). The wetting and drying stages, which can be  
97 expressed by the wet/dry ratio parameter, have a critical impact on the removal rates of dissolved  
98 organic carbon, total nitrogen, and pathogens (Ben Moshe et al., 2020; Morrison et al., 2020;  
99 Sharma and Kennedy, 2017). Although the wet/dry ratio can vary depending on location and  
100 wastewater quality, it is well accepted that it should be below 1.0 (Sattar, 2016; Sharma and  
101 Kennedy, 2017). Nevertheless, infiltration basins behave differently with regard to infiltration  
102 rates and clogging. Thus, in many cases, the SAT operational efficiency is limited to the personal  
103 experience of the operators and their knowledge of the specific infiltration basin (Sharma and  
104 Kennedy, 2017). Note, however, that several studies (e.g., Ben Moshe et al., 2021b) suggest that  
105 it is not the wet/dry ratio that should be considered, but specific times for wetting and drying.

106 The oxidation-reduction potential ( $E_h$ ), together with chemical and physical parameters such as  
107 water content, soil temperature,  $O_2$  concentration, etc., can be continuously monitored by  
108 installing the relevant sensors. Previous studies have implemented the  $E_h$  sensor and successfully  
109 described, with high temporal resolution, the subsurface chemical conditions in various  
110 environments, such as wetlands, the groundwater (or the capillary fringe), aquifers, etc. (Wallace  
111 et al., 2019; McMahon and Chapelle, 2008; Shenker et al., 2005; Silver et al., 2018; Rezanezhad  
112 et al., 2014). To improve SAT system performances, the link between the wetting and drying  
113 stages and the subsequent redox conditions developed in the subsurface should be established.  
114 Thus, in situ monitoring can improve SAT management performance and reduce the subjectivity  
115 of the operator. The objective of this study was to examine the temporal variability in redox  
116 potential and the way it is affected by changes in volumetric water content, gaseous  $O_2$ , and  
117 climate imposed by different operational modes of wetting and drying stages. Furthermore,  
118 calibrated and validated hydrological models were used to explore the behavior of water fluxes  
119 under different operational modes and seasonal temperature changes. Finally, the optimal lengths  
120 of a drying stage and a wetting stage were determined, following the in situ observations.

121

## 122 **2 Methods**

### 123 | **Study sites**

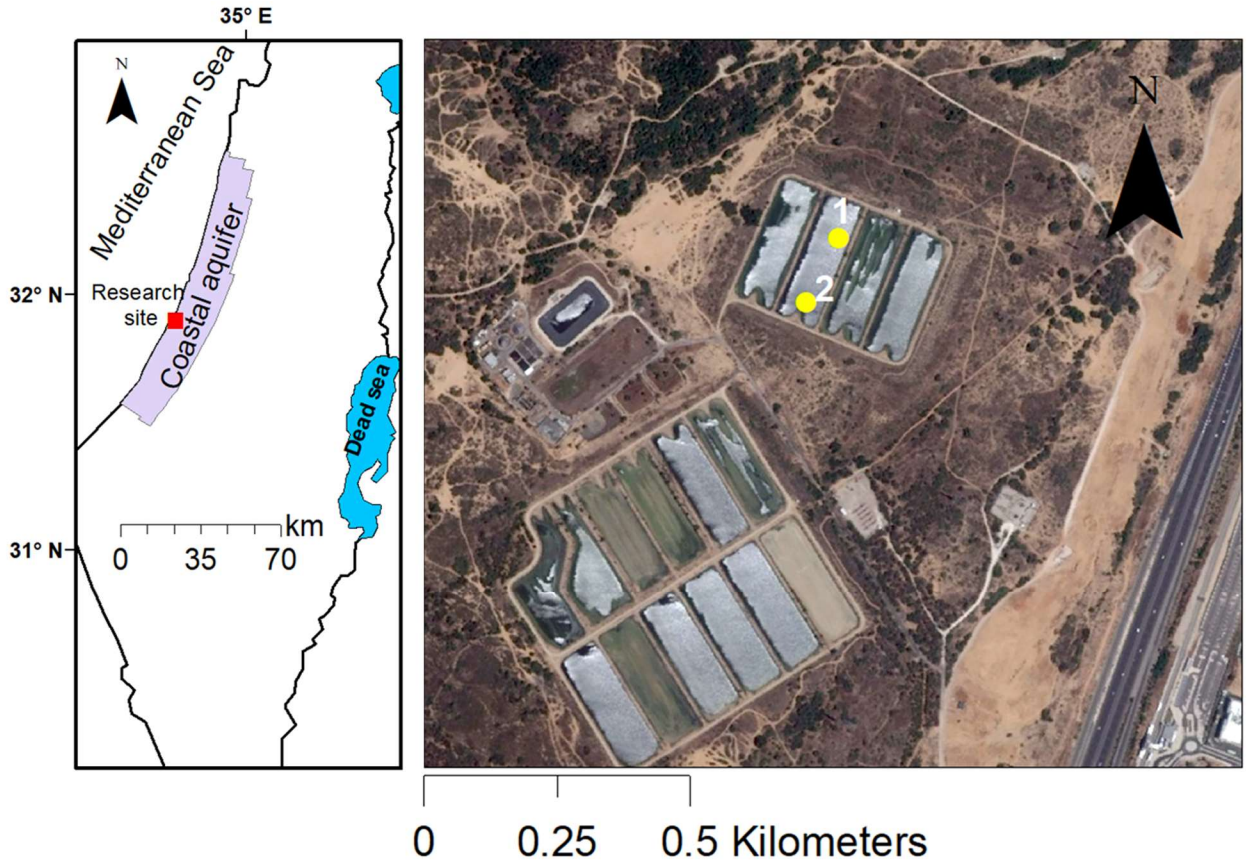
124 The Dan region reclamation project (Shafdan) reclaims about 125 million  $m^3$  of effluent  
125 annually, from the Tel Aviv metropolitan area in Israel. The treatment of effluents occurs in two  
126 stages. The first stage involves mechanical-biological treatment, which is based on activated  
127 sludge, while in the second stage, the treated water (a secondary effluent) is delivered to  
128 infiltration basins, as part of the SAT system, to further improve water quality. Six infiltration  
129 basin sites, covering a total area of 1.053  $km^2$ , are located in central Israel, overlying the coastal  
130 aquifer (Figure 1). Each basin is divided into several spreading ponds, about 1500  $m^2$  each,  
131 which are alternately flooded. The vadose zone that underlies the basins is mostly composed of  
132 sand, sandy loam soil, and calcareous sandstone layers. Typically, the ponds are flooded for one  
133 to two days (max hydraulic head of about 50 cm), followed by two to six days of drainage and  
134 soil surface drying. The wetting and drying stages are controlled by the ponds' flooding order,

135 the availability of effluent, and the drying period, which is suggested to be at least 24 h (Icekson-  
136 Tal et al., 2003). The basin surface is plowed on a regular basis to break up the developed  
137 biocrust and to prevent clogging (see Negev et al. (2020) for details).

## 138 | **Study operation**

139 In this research, two in situ measurement stations were installed in an infiltration pond during  
140 2018 (pond 4103 in the Yavne 1 cluster, Figure 1). Each station was equipped with several sets  
141 of sensors at 25, 50, 75, 100 and 150 cm depth, including time domain transmittance (TDT)  
142 probes (Acclima Inc., Idaho, USA), copper-constantan thermocouples (OMEGA Engineering,  
143 Inc., Connecticut, USA), oxidation-reduction potential (ORP) electrodes (ELH016 van London  
144 Co, Houston, TX, USA), and O<sub>2</sub> percentage probes (ICT02 sensor, ICT Int., Australia). Data  
145 were collected at prescribed intervals and logged on a CR1000 data logger (Campbell Scientific,  
146 Inc., Logan, UT, USA). In addition, suction cups were installed at similar depths. In station 1  
147 (Figure 1), the data consisted of volumetric water content ( $\theta$ ), soil temperature (T), and ORP (E<sub>h</sub>)  
148 time series, which were continuously measured every 20 minutes between 28/07/2020 and  
149 10/02/2021 (total of 14,185 values, 197 days, for each variable). The data were obtained at 25,  
150 50, and 100 cm depths. In station 2 (Figure 1),  $\theta$ , T, gaseous oxygen (O<sub>2</sub>), and E<sub>h</sub> were measured  
151 every 20 minutes between 08/05/2019 and 20/07/2020. There were about 60 days in which data  
152 were not collected in station 2 due to technical issues. The data from station 2 contained 27,222  
153 points of  $\theta$ , 29,394 points of O<sub>2</sub>, 30,414 points of E<sub>h</sub>, and 26,730 points of T measurements. In  
154 station 2, the data were collected at 25, 50, 75 and 100 cm depths.

155 The water quality characteristics of the secondary effluent that flooded the Yavne 1 basin are  
156 presented in the *Supporting Information* (Fig. S1). Note that the quality parameter concentrations  
157 conform to the updated “Inbar” regulations (Inbar, 2007) and the findings of a previous study  
158 that surveyed numerous wastewater storage and treatment reservoirs across the country (Kfir et  
159 al., 2012). To determine the soil physical properties, undisturbed soil cores were sampled at  
160 different depths. Subsequently, flow experiments were carried out to calculate the saturated  
161 hydraulic conductivity ( $K_s$ ) based on Darcy's Law (*Supporting Information*, Fig. S2).  
162 Additionally, particle size distribution (PSD) analyses are presented in Fig. S3 (*Supporting*  
163 *Information*). The PSD results indicate that the SAT vadose zone is homogeneous.



164

165 Figure 1: *The location of the investigated site, the Yavne 1 infiltration basin of the Shafdan.*  
 166 *In the close up of the investigated pond, the yellow circles represent the locations of the*  
 167 *measurement stations (©Google Earth).*

168

169 | **Hydrological model and gaseous oxygen dynamics**

170 The calculations for water and oxygen fluxes in the SAT vadose zone are calculated differently  
 171 for the ponding stage and for the stage where there is no ponding (water) on the soil surface. For  
 172 the ponding stage, Ganot et al. (2017) showed that the infiltration rates in managed aquifer  
 173 recharge systems can be predicted reasonably well by simple analytical models. In this study, the  
 174 Green-and-Ampt equation for infiltration into a flooded soil was implemented to calculate the  
 175 water flux (Bouwer, 2002):

176 
$$q = Ks \times \frac{(L + d - \psi^*)}{L} \quad (1)$$

177 where  $q$  ( $L T^{-1}$ ) is the water flux,  $d$  ( $L$ ) is the ponding depth,  $L$  ( $L$ ) is the thickness of the  
 178 saturated vadose zone, and  $\psi^*$  ( $L$ ) is the negative pressure head at the wetting front. Note that  $L$   
 179 is assumed here to be constant, the subsurface is assumed to be homogeneous, and  $\theta$  is assumed  
 180 to vary with time only. As the wetting front progresses, the gradient approaches a value of unity,  
 181 and the infiltration rate becomes equal to the hydraulic conductivity of the wetted zone. Once the  
 182 water ponding ceases, the water drainage is set equal to the unsaturated hydraulic conductivity,  
 183 described with an exponential form (Guswa et al., 2002):

$$184 \quad D(\theta) = K_s \frac{e^{\beta(\theta - \theta_{fc})} - 1}{e^{\beta(\theta_s - \theta_{fc})} - 1} \quad (2)$$

185 where  $K_s$  ( $L T^{-1}$ ) is the saturated hydraulic conductivity,  $\beta$  is a parameter of the soil,  $\theta$  ( $L^3 L^{-3}$ ) is  
 186 the volumetric water content,  $\theta_{fc}$  ( $L^3 L^{-3}$ ) is the water content at field capacity, and  $\theta_s$  ( $L^3 L^{-3}$ ) is  
 187 the saturated water content. Furthermore, the effect of temperature changes on the soil hydraulic  
 188 conductivity is implemented through the change in viscosity (Lin et al., 2003):

$$189 \quad K_{sT} = K_{s25} \frac{\mu_{25}}{\mu_T} \quad (3)$$

190 where  $K_{sT}$  and  $K_{s25}$  are soil hydraulic conductivity values at temperature  $T^\circ C$  and  $25^\circ C$ ,  
 191 respectively, and  $\mu_T$  and  $\mu_{25}$  are the dynamic viscosity of water ( $M L^{-1} T^{-1}$ ) values at  $T^\circ C$  and  $25^\circ$   
 192  $C$ , respectively.

193 An inverse problem was set to find an optimal combination of  $K_s$  and  $\beta$  parameters that  
 194 minimizes the following objective function:

$$195 \quad \Phi(b) = \sum_{i=1}^N [\theta(t_i) - \theta(t_i, b)]^2 \quad (4)$$

196 where  $N$  is the number of the  $\theta$  observations,  $\theta(t_i)$  are the observations at a specific time, and  
 197  $\theta(t_i, b)$  are the corresponding models' (Eq. 1 to 3) predictions for the vector of optimized  
 198 parameters,  $b$  ( $K_s$  and  $\beta$ ). The inverse problem was solved using the *fminsearch* function in  
 199 MATLAB. To evaluate the prediction quality, the root mean squared error (RMSE), the Nash



200 Sutcliffe efficiency (NSE), and the Pearson correlation ( $r$ ) were calculated following Ritter &  
201 Muñoz-Carpena (2013).

202

### 203 **3 Results and Discussion**

204 The water level measurements at the soil surface were collected by the Shafdan operators as part  
205 of the operational routine. Analysis of the water level data (ponding depth) indicates two  
206 operational modes of long and short cycles that were implemented at the investigated pond. The  
207 characteristics of the drying and wetting stages, as recorded by the operators, are summarized in  
208 Table 1. Note that the wetting stage is defined when water is present at the soil surface and the  
209 drying stage is defined when water is absent. Further note that the water level is measured at a  
210 single point (close to the pond inlet). Therefore, some variations, at the order of a few cm, may  
211 exist due to microtopography and the distance between the inlet and the far parts of the pond.  
212 This may lead to some delays in water arrival or recession from the stations. Throughout the  
213 analysis described below, we define the winter period as the months between November and  
214 April and the summer period as the months between May and October, corresponding to the  
215 Mediterranean climate. Our monitoring systems are operated independently from the Shafdan  
216 facilities.

217 **Table 1.** Technical information of the recorded long and  
218 short wetting and drying cycles (this data was provided by  
219 the Shafdan operators).

	Long cycles	Short cycles
Wetting stage (days)	$9 \pm 2.4$	$1.5 \pm 0.4$
Drying stage (days)	$3.3 \pm 2.4$	$1.8 \pm 1$
Number of recorded cycles	33	37
Length of cycle (days)	$12.7 \pm 3$	$3.2 \pm 1.3$
Wet/dry ratio	$3 \pm 1.8$	$0.9 \pm 0.3$

220

### 221 | **Hydrological conditions**

222 A representative set of  $\theta$  time series measured in the SAT's vadose zone is presented to describe  
223 the variability in hydrological conditions measured throughout different seasons and operational  
224 modes (Figure 2). The  $\theta$  measurements were obtained during long (Figure 2a, b, c) and short  
225 (Figure 2d) cycles at three different depths. Note that the water content measurements presented  
226 in Figure 2 (a, b) were recorded at station 2 (Figure 1), during summer (Figure 2a) and winter  
227 (Figure 2b). The water content variations under short cycles were measured at station 1 (Figure  
228 2c, d). Differences in the absolute values between the water content observations at different  
229 depths are mainly related to the vertical texture variability (Fig. S2, *Supporting Information*).  
230 Under the long cycles,  $\theta$  measurements were obtained throughout 19 cycles during summer  
231 (May–October) and 14 cycles during winter (November–April). Under short cycles, there were  
232 12 cycles during summer and 25 during winter.

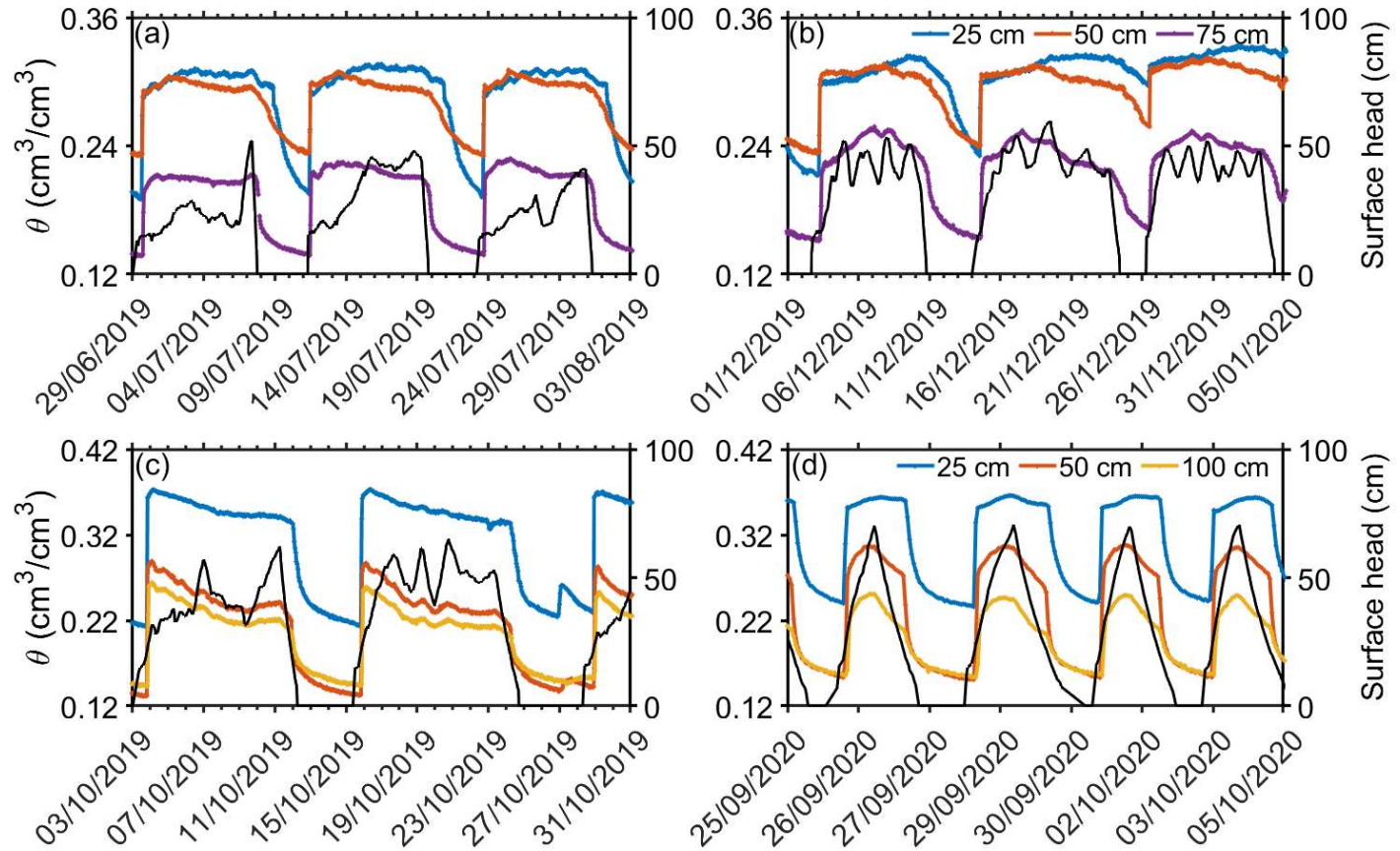
233 Every recorded wetting event prompted an intensive infiltration that was expressed by a rapid  
234 and almost instantaneous increase in water content at all depths and under the two operational  
235 modes (Figure 2). Furthermore, the soil remained at similar level of saturation throughout each  
236 wetting stage. Similarly, once the drying process started, it occurred virtually simultaneously at  
237 all depths. There were noticeable differences in the drainage rates between summer and winter,  
238 where the soil dried faster in summer. To elaborate the drainage process, the drying stages were  
239 assembled and averaged at an hourly interval and separated into short (Figure 3a) and long  
240 (Figure 3b) cycles. Additionally, Eq. (1), (2), and (3) (the hydrological model) were implemented  
241 to describe the water flow in the SAT's vadose zone under long and short cycles. The  
242 hydrological models were calibrated and validated against water content observations at 25 cm  
243 depth by adjusting the  $K_s$  and  $\beta$  parameters (Fig. S4 and Fig. S5, *Supporting Information*, Table  
244 2). Throughout the calibration, the  $K_s$  and  $\beta$  parameters attained different values for the long  
245 cycle periods and the short cycle periods (Table 2). There are differences in soil physical  
246 properties between stations 1 and 2, which explains the need for calibrating different parameter  
247 sets. In addition, the calibrated  $K_s$  values for both models were substantially lower than the  
248 measured  $K_s$  values (Fig. S2, *Supporting Information*, Table 2). It has been shown that  $K_s$   
249 measurements in the field are commonly lower than lab  $K_s$  measurements (Nimmo et al., 2009).  
250 This is related to a reduction in soil conductivity due to air trapping in the soil pores during the  
251 wetting process when water is applied at the land surface (Mizrahi et al., 2016; Nimmo et al.,  
252 2009).

253 Under the short cycles, the soil drainage process occurred mostly within the first 15 hours of the  
254 drying stage (Figure 3a). The soil drainage rate was slightly higher in summer than in winter.  
255 Under the short cycles, the model successfully followed the observed trends, where the  
256 validation period showed similar performances (Fig. S4 and Figure 3a). The model results for the  
257 short cycles confirm that the differences in drainage between summer and winter are mainly due  
258 to temperature changes that affect water viscosity (Lin et al., 2003). During the long cycle  
259 application, the drainage rates in summer showed a moderate  $\theta$  decline compared to the observed  
260  $\theta$  under short cycles (Figure 3b). This might be due to the differences in soil physical parameters  
261 between stations 1 and 2, as highlighted by the calibrated models' parameters (Table 2).

262 While the model under long cycles successfully followed the drainage trend during summer, the  
263 model showed poor performance during winter under long cycles. This is mainly due to the  
264 observable changes in  $\theta$  measurements, which displayed a shift towards higher values from  
265 November 2019 (Fig. S5 and Figure 2b). To explore the changes in the SAT's physical  
266 properties, an additional parameter set was calibrated against the winter data only during the long  
267 cycles (Figure 3b, green line). Both the  $K_s$  and  $\beta$  parameters attained lower values, and the  $\theta_s$   
268 increased (Fig. S6 and Table 2). Previous studies related the accumulation of organic matter in  
269 SAT to lower rates of organic matter decomposition during winter (Nadav et al., 2012a, b; Arye  
270 et al., 2011). The authors ruled out the occurrence of soil clogging and indicated that the  
271 accumulation of organic matter at the topsoil increased the degree of soil water repellency or soil  
272 hydrophobicity. This phenomenon often develops in sandy soils (commonly used in SAT) due to  
273 the low specific surface area of sand ( $\sim 0.0077 \text{ g m}^{-2}$ ) compared to clay ( $\sim 900 \text{ g m}^{-2}$ ) (Doerr et al.,  
274 2000; Wallis and Horne, 1992). Thus, only a small amount of organic matter is required to coat  
275 the particles of the sand in order to develop soil water repellency (Wallis and Horne, 1992). Arye  
276 et al. (2011) showed that soil hydrophobicity is attributed to the reduction of liquid surface  
277 tension and increase of the contact angle. These changes in soil properties are related to the  
278 reduction of the soil permeability (Nadav et al., 2012b). It appears that long wetting and drying  
279 cycles in SAT during winter can alter the physical soil properties, which eventually affect the  
280 infiltration capabilities.

281

282



283  
 284 Figure 2: Representative time series of  $\theta$  measurements obtained at station 2 (Figure 1) during (a) summer  
 285 and (b) winter under long wetting and drying cycles at three different depths. Black line represents the  
 286 surface water hydraulic head. The bottom plots display  $\theta$  measurements obtained at station 1 under (c)  
 287 long and (d) short wetting and drying cycles during the summer.

288

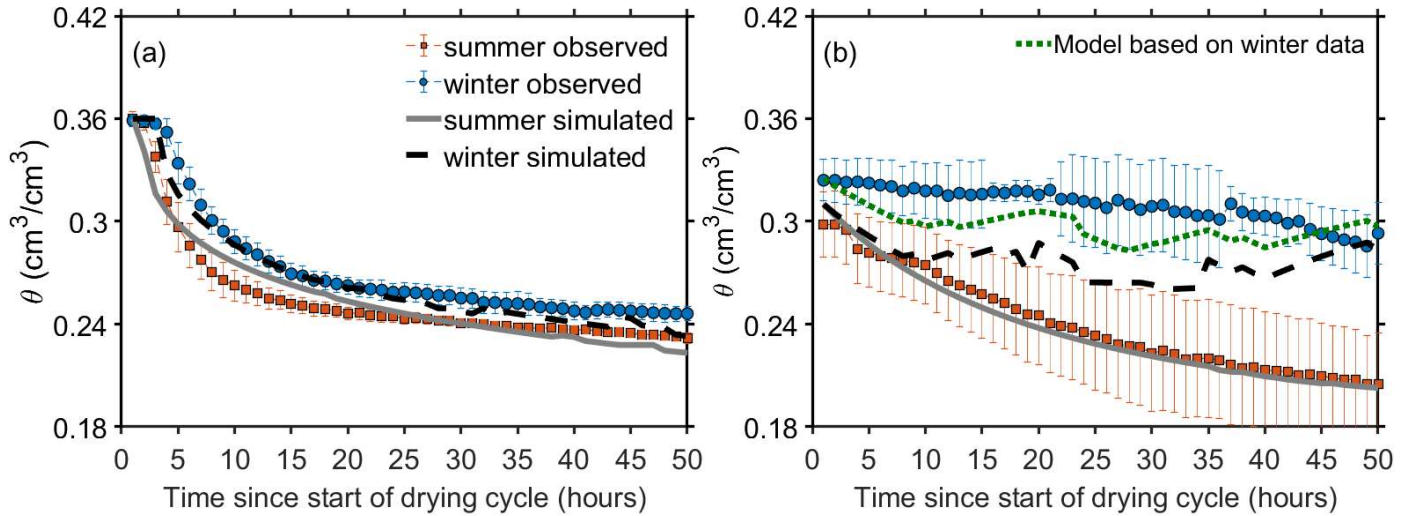
289

**Table 2.** Estimated parameters of the hydrological models

	Station 1	Station 2	Station 2 (winter only)
$Ks$ (cm h <sup>-1</sup> )	<b>5</b>	<b>0.9</b>	<b>0.72</b>
$\theta_s$	0.36	0.32	<b>0.33</b>
$\beta$	<b>30</b>	<b>6.75</b>	<b>6.48</b>
$\theta_{fc}$	0.19	0.19	0.19
$\psi^*$ (cm)	-15	-15	-15

$\theta_h$                       0.05                      0.05                      0.05

290



291

292 Figure 3: The average and standard deviation values of measured  $\theta$  at 25 cm depth throughout  
 293 the drying stages at an hourly time scale: (a) short cycles (station 1) and (b) long cycles (station  
 294 2). The blue and red circles represent the average  $\theta$  values collected during winter (November–  
 295 April) and summer (May–October), respectively. The statistics of measured  $\theta$  under long cycles  
 296 are based on 19 drying stages during summer and 14 drying stages during winter. For the short  
 297 cycles, the statistics are based on 12 drying stages during summer and 24 drying stages during  
 298 winter. The dashed black and solid gray lines represent the average values of simulated  $\theta$   
 299 throughout the drying stage during winter (November–April) and summer (May–October),  
 300 respectively. Note that for the long cycle periods, an additional model was established based  
 301 only on winter data (green line).

302

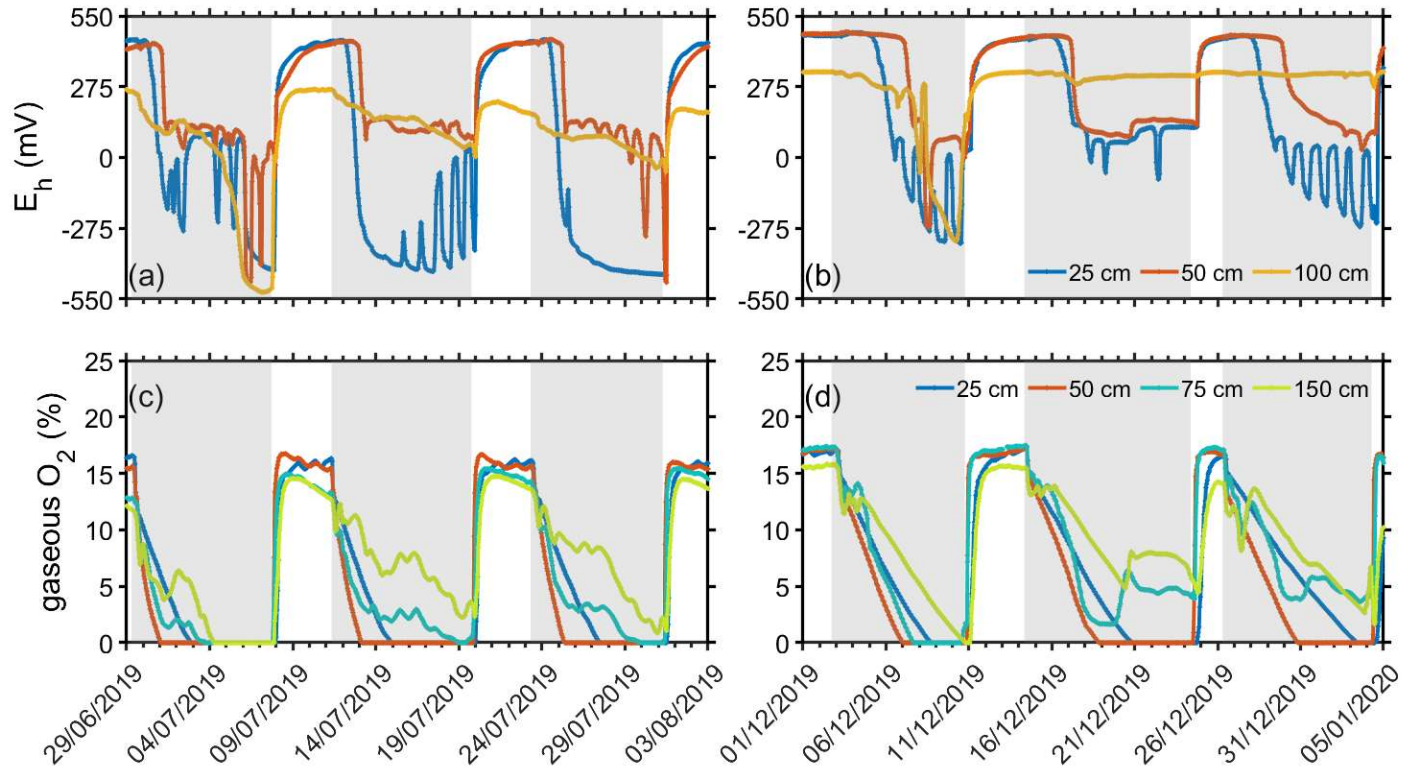
303 | **Seasonal differences in SAT redox ( $E_h$ ) conditions under long wetting cycles**

304  $E_h$  conditions were monitored at four depths (Figure 4a, b). The behavior of the  $E_h$  dynamic  
 305 following a wetting event was similar for the summer and the winter periods. At 25, 50, and 75  
 306 cm depths, a gradual decline in  $E_h$  started only after a time lag from the beginning of a wetting  
 307 event (Figure 4a, b). This time lag can be explained by the presence of dissolved oxygen (DO) in  
 308 the percolating solution. Once DO is depleted, suboxic and anoxic conditions begin to develop

309 (Dutta et al., 2015; Ben Moshe et al., 2021, 2020). The  $E_h$  conditions at 25 cm were the most  
310 highly responsive to the wetting events, while the  $E_h$  conditions were the most negative at this  
311 depth (Figure 4a, b). At 100 cm depth, only minor changes were observed, and in some cases  
312 (during winter), no changes were observed (Figure 4a, b). According to the gaseous  $O_2$   
313 measurements (Figure 4c, d), there were partially aerated conditions (unsaturated conditions)  
314 during some of the flooding events at 75 cm depth, while at 150 cm depth, unsaturated  
315 conditions prevailed continuously throughout the period of measurements. Therefore, the small  
316 changes of  $E_h$  at 100 cm depth could either have been the outcome of only minor biochemical  
317 activity, or they could have been due to the sufficient oxygen supply. Gorski et al. (2019)  
318 suggested that in coarse-grained soils, due to the high infiltration rates, the DO is delivered  
319 rapidly by the percolating water to the base of the saturated zone. Thus, the soil microbes do not  
320 have enough time to consume the DO. In the current study it is reflected by positive  $E_h$  values at  
321 100 cm depth (Figure 4a,b). As the wetting cycle continues, the  $E_h$  conditions at 100 cm depth  
322 decrease, mainly during summer (Figure 4a,b). This indicates that eventually the infiltrated water  
323 that reaches 100 cm depth contains lower concentrations of DO. Yet, the  $E_h$  conditions do not  
324 show further decrease, which can be attributed to limited microbial activity. Previous studies  
325 showed that carbon availability at greater depths of the vadose zone is a dominant factor for this  
326 limitation (Grau-martínez et al., 2018, 2017; Brettar et al., 2002). Furthermore, the monitored  $E_h$   
327 conditions illustrate that most of the activity in SAT systems occurs at the topsoil, as illustrated  
328 in previous studies (e.g., Quanrud et al., 1996, 2003; Sopilniak et al., 2017; Grinshpan et al.,  
329 2022). Note that the  $E_h$  recovery time, i.e., an increase towards positive values, was virtually  
330 instantaneous once the drying process initiated (Figure 4a, b). The increase in  $E_h$  conditions  
331 occurred concurrently with the observed rapid increase of the gaseous oxygen ( $O_2$ ) in the vadose  
332 zone (Figure 4c, d).

333 A distinct difference in  $E_h$  conditions between winter and summer at 25 cm depth is expressed by  
334 a more negative range of values during summer (Figure 4a, b). Since similar wastewater quality  
335 and hydraulic loads were fed to the pond during summer and winter (*Supporting Information*),  
336 the  $E_h$  conditions were mainly affected by the SAT's aeration state and seasonal temperature  
337 changes. In Figure 5, the monthly  $E_h$  conditions at 25 cm depth are presented in the form of a  
338 boxplot, together with the monthly average ambient temperature (dashed black line) and monthly  
339 average global radiation (gray line). The  $E_h$  conditions showed a wider range of values with the

340 increase in temperature (Figure 5). Between November and March, the  $E_h$  conditions mostly  
341 remained above zero or were slightly negative (Figure 5). Once the temperature increased above  
342  $24^\circ\text{C}$  between May and October,  $E_h$  conditions showed substantial fluctuation between negative  
343 and positive values (Figure 5). Note that the average monthly ambient temperatures during  
344 November and May were similar in value, but during November, the  $E_h$  conditions mostly  
345 remained above zero (Figure 5). This difference is connected to the daylight duration, as  
346 indicated by the global radiation, which is substantially greater in May than in November (Figure  
347 5, gray line). A typical characteristic of aquatic systems is the large fluctuations in dissolved  
348 oxygen (DO) concentrations due to intense photosynthesis and respiration (Stumm and Morgan,  
349 1996). Goren et al. (2014) illustrated that following the effluent spreading in the infiltration  
350 ponds, photosynthesis enriches the water with DO. Furthermore, chemical analysis of porewater  
351 samples that were obtained at 0.5 m depth in the SAT vadose zone indicated DO's substantial  
352 influence on the biochemical conditions of the percolating water (Goren et al., 2014). Thus, the  
353 photosynthesis process enriches the effluent with DO, which encourages further microbial  
354 activity (Goren et al., 2014; Hargreaves, 2006; Rodríguez-Escapes et al., 2020). However,  
355 between July and September, there was a decrease in global radiation that did not affect the  $E_h$   
356 variability (Figure 5). Thus, it appears that under long wetting stages, the seasonal temperature  
357 changes dominate the  $E_h$  conditions but show some trade-off with the global radiation.

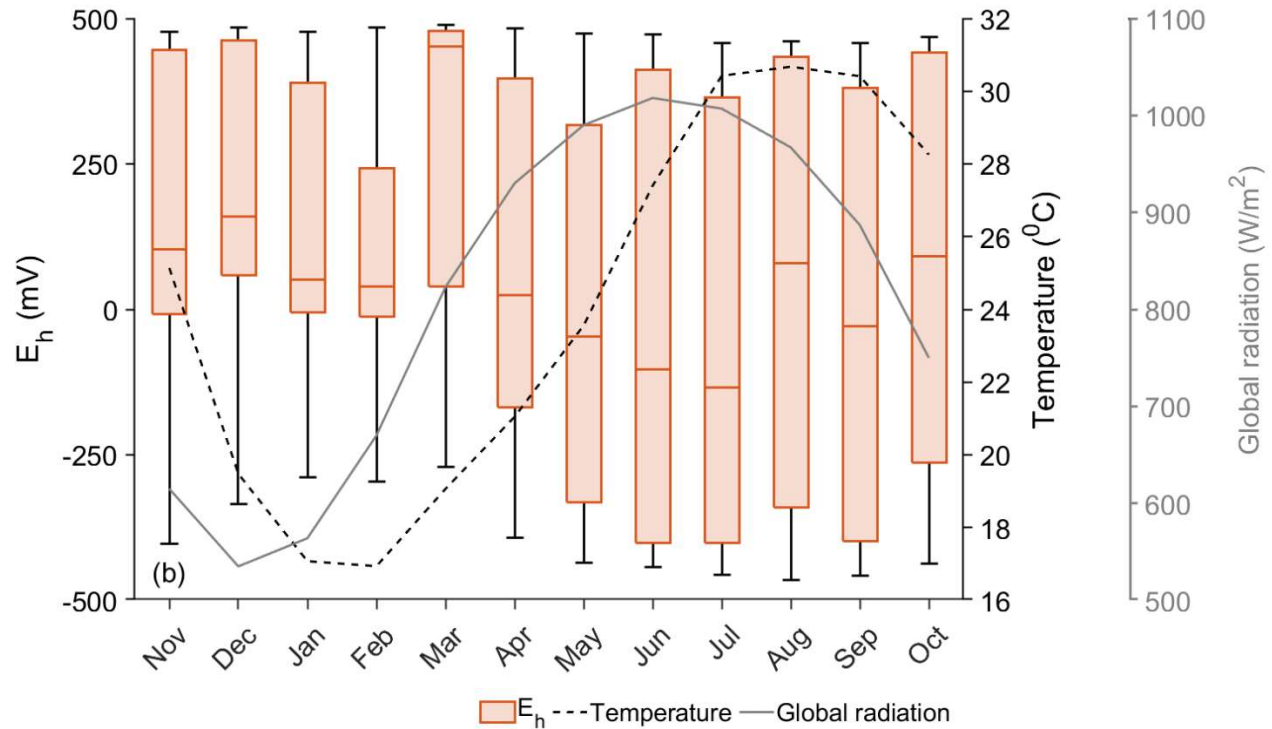


358

359 Figure 4: Representative time series of redox-potential ( $E_h$ ) and gaseous  $O_2$  measurements  
 360 obtained at station 2 (Figure 1) at depths of 25, 50, and 100 cm: (a, c) summer and (b, d) winter.  
 361 Note that the gray and white areas indicate wetting and drying periods, respectively.

362





363

364 Figure 5: Seasonal changes in  $E_h$  conditions as were observed at 25 cm depth at station 2 under  
 365 long (seven days) wetting periods. The dashed black line represents the monthly mean ambient  
 366 temperature, and the solid gray line represents the monthly mean global radiation obtained from  
 367 the Israeli Meteorological Service (IMS, 2021).

368

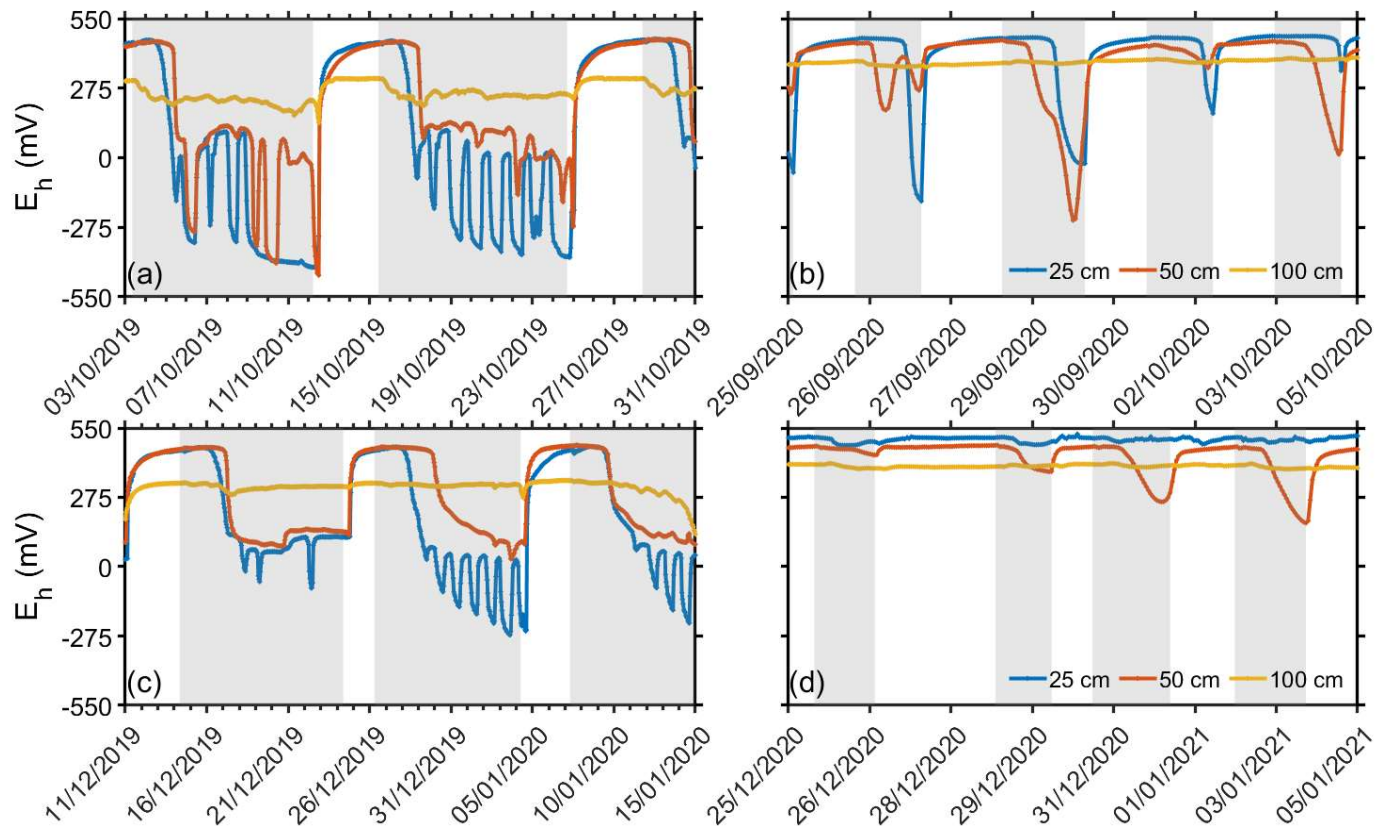
### 369 | A comparison between SAT redox ( $E_h$ ) conditions under long and short cycles

370 It has been shown that the operational mode affects the aeration conditions of the upper vadose  
 371 zone, which consequently might alter the infiltration rates and the intensity of the  
 372 biogeochemical processes (Goren et al., 2014). Throughout the measurement period, the  
 373 intervals of wetting and drying stages were modified (Table 1). The wetting and drying stages  
 374 were substantially shortened during September 2020, which enabled examining the differences in  
 375  $E_h$  conditions under short and long cycles. The variations in  $E_h$  conditions under long cycles  
 376 during October 2019, December 2019, and January 2020 are presented in Figure 6a, c. In  
 377 addition, the changes in  $E_h$  conditions under short cycles during September–October 2020,  
 378 December 2020, and January 2021 are presented in Figure 6b, d.

379 As was shown above, under long cycles, the  $E_h$  conditions declined towards slightly negative  
380 values during winter and attained markedly negative values during the summer months at 25 and  
381 50 cm depths, where only minor variations were observed at 100 cm depth (Figure 6a, c). The  $E_h$   
382 conditions, under short cycles during the summer, showed a decline towards slightly negative  
383 values for a brief time compared to long cycles (Figure 6a, b). During the winter, only minor  
384 variations in  $E_h$  conditions were recorded under short cycles (Figure 6d). Note that at 100 cm  
385 depth, there was almost no change in  $E_h$  conditions for either season under short cycles (Figure  
386 6b, d). As was illustrated previously (Figure 4a, b), once the drying stage initiated, the recovery  
387 of  $E_h$  towards positive values (oxic conditions) was almost instant under both short and long  
388 cycles. It appears that the re-establishment of oxic conditions occurs independently of the length  
389 of the wetting stage.

390 The observations of  $E_h$  and gaseous  $O_2$  under long and short cycles indicate a weak relationship  
391 between the wetting and the drying stages. These results call into question the advantage of  
392 implementing the wet/dry ratio for optimizing SAT performance. It appears that the length of a  
393 wetting stage and a drying stage should be defined separately (Ben Moshe et al., 2020, 2021).  
394 Thus, the necessary further investigation is described below to examine the optimal lengths of  
395 the wetting and drying stages.

396



397  
 398 Figure 6: Representative time series of redox-potential ( $E_h$ ) measurements at 25, 50 and 100 cm depths in  
 399 station 1 (Figure 1): (a, c) long wetting periods and (b, d) short wetting periods. Note that the gray and  
 400 white areas indicate wetting and drying periods, respectively.

401

402 | **The length of the wetting stage according to  $E_h$  measurements**

403 During wetting stages, the main limiting factor of the biodegradation process is the availability  
 404 of dissolved oxygen (Skopp et al., 1990; Cook and Knight, 2003). Once the soil pores are fully  
 405 saturated, only the dissolved oxygen (DO) of the percolating water is available. However, studies  
 406 have illustrated that the DO of the percolating water rapidly depletes (Dutta et al., 2015; Ben  
 407 Moshe et al., 2021, 2020). Thus, the wetting stage should cease when the DO no longer has an  
 408 effect on the degradation process, i.e., when suboxic and anoxic conditions begin to develop.  $E_h$   
 409 measurements can provide a good indication for the time when such conditions begin to be  
 410 established. For this purpose, the hourly measured  $E_h$  conditions during the wetting stage of 33  
 411 recorded cycles (19 cycles during summer and 14 cycles during winter) were averaged for 25,

412 50, 75 and 100 cm depth (Figure 7). The data were separated between winter (November–April)  
413 and summer (May–October), according to the trends presented in Figure 5.

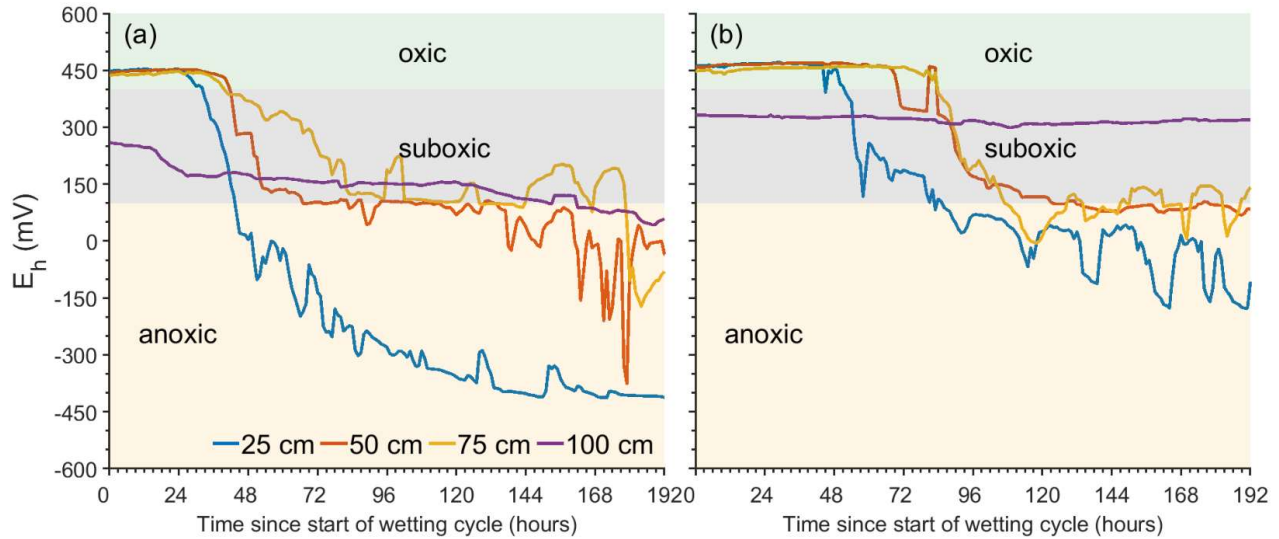
414 During summer, the decline in  $E_h$  conditions were steeper compared to the trends exhibited in  
415 winter (Figure 7). Following 30 hours of wetting, the  $E_h$  conditions during the summer dropped  
416 below 400 mV at 25 cm depth, which indicates the establishment of suboxic conditions (Figure  
417 7a). After 37 hours, the  $E_h$  observations at 50 and 75 cm depths showed similar trends (Figure  
418 7a). Note that after 45 hours the  $E_h$  observations at 25 cm depth reach anoxic conditions. The  
419 differences between  $E_h$  measurements at topsoil and at deeper parts of the vadose zone were  
420 previously attributed to carbon availability, which decrease with depth (Brettar et al., 2002;  
421 Bohrerova et al., 2004). Furthermore, Brettar et al. (2002) provided a range of threshold  $E_h$   
422 values for denitrifying conditions depending on the depth of the soil horizon. Similarly, despite  
423 the differences between the  $E_h$  measurements at 25 cm depth and at deeper depths (Figure 7), all  
424 the  $E_h$  measurements potentially indicate similar activity. To prevent anoxic conditions in the  
425 SAT vadose zone during summer, the optimal length of a wetting stage, in terms of  
426 biodegradation, would be about 30 hours (1.25 days). This is in agreement with Dutta et al.  
427 (2015), who suggested a relatively wide distribution of de-oxygenation times, between 0.36 and  
428 1.5 days.

429 In winter, the  $E_h$  measurements decrease towards suboxic conditions, that occur after 51, 69 and  
430 84 hours of wetting at 25, 50 and 75 cm depths, respectively (Figure 7b). The delay in  $E_h$  drop  
431 (compared to summer) is partly explained by the longer presence of gaseous  $O_2$  in the SAT  
432 vadose zone (Figure 4c,d and Figure 8). It takes a longer time for the gaseous  $O_2$  to deplete  
433 during winter (Figure 8), probably as a result of lower oxygen demand due to slower microbial  
434 activity at low temperatures (Kirschbaum, 1995). An additional explanation for the longer  
435 presence of gaseous  $O_2$  is due to longer establishment of saturated conditions as a consequence of  
436 lower  $K_s$  values (see section *Hydrological conditions*). However, once the gaseous  $O_2$  is absent  
437 from the SAT vadose zone during winter (Figure 8), no further decrease in  $E_h$  conditions occur  
438 (Figure 7b). Therefore, the trade-off between nutrient transport rates and reaction rates should be  
439 considered, where the supply of the percolated effluent's substrate might be faster than the  
440 SAT's degradation capability (Greskowiak et al., 2006). Determining the length of a wetting  
441 stage during winter, using solely the  $E_h$  and gaseous  $O_2$  measurements, may be challenging.

442 Nevertheless, the changes in soil physical parameters and the seasonal differences in  $E_h$  values  
443 imply low biodegradation rates during winter. From a practical perspective, the observed  $E_h$   
444 values at 25 cm depth during winter are compared with the  $E_h$  measurements during summer.  
445 Using a two-sample t-test show that the differences in the first 28 hours of a wetting cycle are  
446 insignificant. It suggests that the length of a wetting stage during winter should be no more than  
447 30 hours, as in the summer period. Nevertheless, given the evidences that are reflected in the  
448 measurements of the current study and conclusions from previous studies, the implementation of  
449 SAT during winter is questionable. It might be necessary to store the effluents in reservoirs  
450 during winter and apply the SAT during summer.

451 According to the  $E_h$  sensor at 100 cm, suboxic conditions prevail for most times during winter  
452 and a moderate decrease (compared to the other sensors) in  $E_h$  conditions is noticeable during  
453 summer (Figure 7). The gaseous  $O_2$  observations at 75 cm indicate depletion of gaseous  $O_2$   
454 during summer and a very low  $O_2$  concentration (2%) during winter (Figure 8c). At 150 cm, the  
455 gaseous  $O_2$  observations suggest that for most of the recorded wetting cycles, unsaturated  
456 conditions prevailed (Figure 8d). It is not clear if the  $E_h$  conditions at 100 cm are determined by a  
457 continuous supply of oxygen given the unsaturated conditions. This might affect the decision  
458 concerning the optimal length of a wetting cycle. However, previous studies (Miller et al., 2006;  
459 Fox et al., 2005; Lin et al., 2008; Goren et al., 2014; Sopilniak et al., 2018; Essandoh et al., 2013;  
460 Quanrud et al., 1996, 2003) and a recent study by our group (Grinshpan et al., 2022) suggest that  
461 most biodegradation activity occurs at topsoil and there is a steep reduction in removal  
462 capabilities with depth. Thus, the potential contribution of the deeper vadose zone to the SAT  
463 treatment should be further investigated.

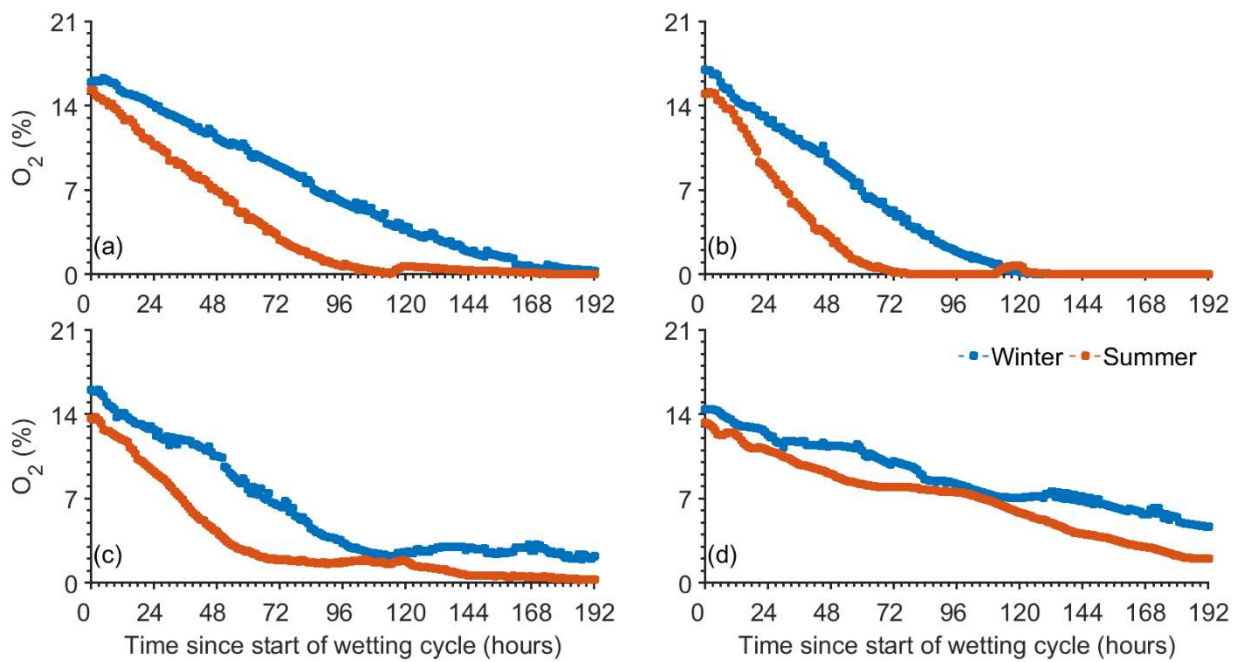
464



465

466 Figure 7: Plot of hourly means of  $E_h$  measurements obtained at station 2, from the beginning of  
 467 the wetting stages at three depths. The statistics are based on 19 cycles during summer (May–  
 468 October) and 14 cycles during winter (November–April) that were observed at (a) winter and (b)  
 469 summer. Note that the data are separated between summer and winter according to the trends  
 470 presented in Figure 5. The green, grey, and yellow areas represent the oxic ( $400\text{mV} <$ ), suboxic  
 471 ( $400\text{mV} > E_h > 100\text{mV}$ ), and anoxic  $E_h < 100\text{mV}$ ) conditions, respectively.

472



473

474 Figure 8. *Plot of hourly means of gaseous O<sub>2</sub> measurements from the beginning of the wetting*  
475 *stages at (a) 25, (b) 50, (c) 75 and (d) 150 cm depths. The statistics are based on 14 cycles*  
476 *during winter (November–April) and 19 cycles during summer (May–October) that were*  
477 *observed at multiple depths in station 2. Note that the data are separated between summer and*  
478 *winter according to the trends presented in Figure 5.*

479

#### 480 | **The length of the drying stage using E<sub>h</sub> and gaseous O<sub>2</sub> measurements**

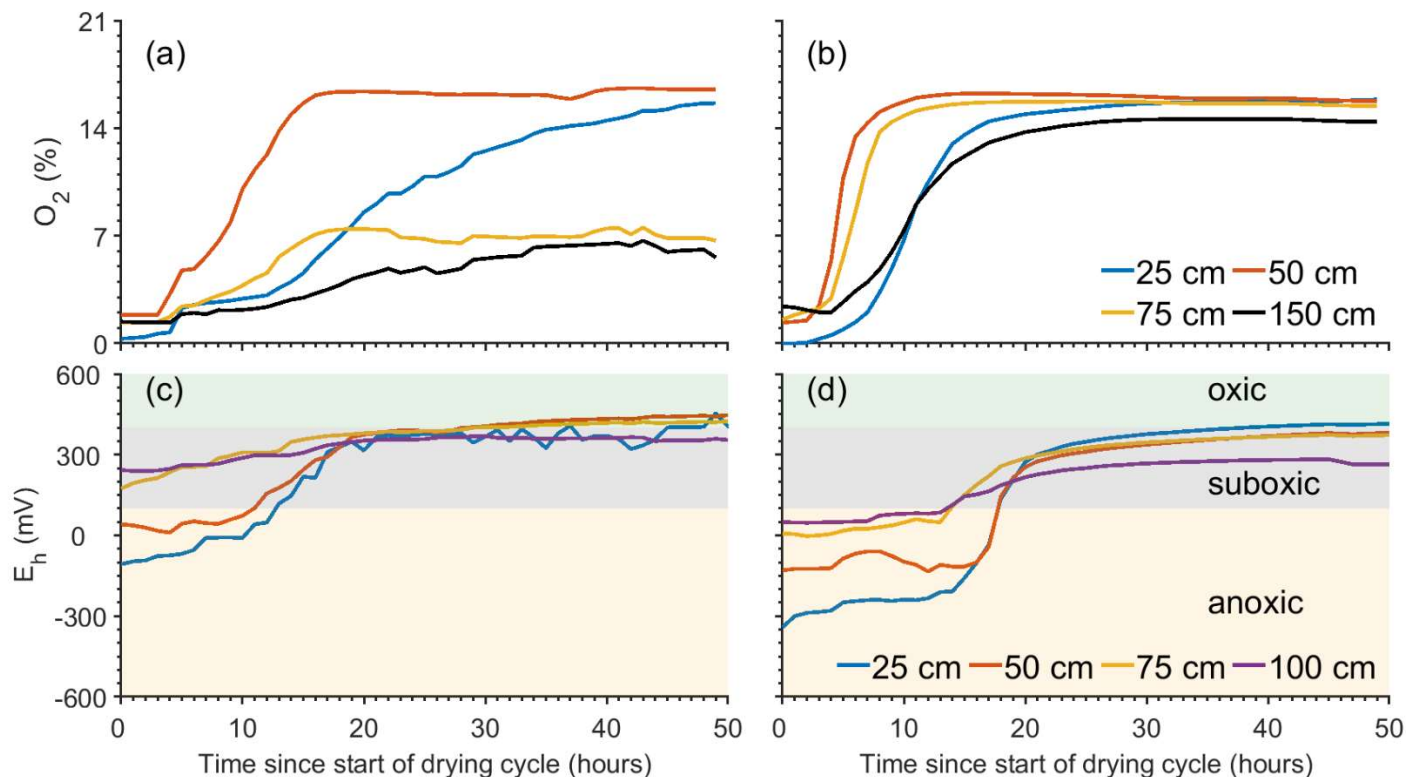
481 The drying stage in SAT systems is implemented to restore the infiltration, biological, and  
482 chemical capabilities of the pond, mainly by aerating the soil (Sharma and Kennedy, 2017). A  
483 drying stage is defined as the stage in which there is no water at the soil surface, and the  
484 observed volumetric water contents begin to decrease (Figure 2). To determine the optimal time  
485 for a drying stage, both the averaged values of the E<sub>h</sub> (Figure 9a,b) and gaseous O<sub>2</sub> (Figure 9c,d)  
486 observations during the drying stages are presented. Note that the E<sub>h</sub> measurements were  
487 conducted at 25, 50, 75 and 100 cm depths and the O<sub>2</sub> observations were obtained at 25, 50, 75  
488 and 150 cm depths (Figure 9). The E<sub>h</sub> and O<sub>2</sub> data during the drying stages were separated  
489 between winter (November–April) and summer (May–October), according to the trends  
490 presented in Figure 5.

491 Slower aeration rates and larger variability were observed during winter compared to summer  
492 (Figure 9a,b). Furthermore, the E<sub>h</sub> recovery is clearly dominated by the rates of the gaseous O<sub>2</sub>  
493 intrusion to the soil (Figure 9c,d). During winter, the aeration rates are different at each depth,  
494 but in general the gaseous O<sub>2</sub> concentrations increase moderately with time (Figure 9a). The  
495 recovery of the E<sub>h</sub> conditions display comparable trends (Figure 9c). Although the O<sub>2</sub> sensor at  
496 50 cm depth suggest a faster O<sub>2</sub> intrusion rate compared to the other sensors (Figure 9a), it is not  
497 expressed in the E<sub>h</sub> recovery time (Figure 9c). During summer all the observed O<sub>2</sub> curves show  
498 steep recovery that ceases after about 20 hours (Figure 9b). According to the O<sub>2</sub> observations, the  
499 gaseous O<sub>2</sub> intrusion process at 50 and 75 cm depths starts at the very beginning of the drying  
500 stage, while at 25 and 100 cm depths there is a two-hour delay (Figure 9b). Nevertheless, the E<sub>h</sub>  
501 conditions recovery is comparable at all depths (Figure 9d).

502 The  $E_h$  observations illustrate that the re-establishment of oxic conditions in the SAT vadose  
 503 zone is similar during winter and summer (Figure 9c,d). Once the drying stage started, it required  
 504 about 36 hours for the  $E_h$  conditions to reach values in the range of oxic conditions, regardless of  
 505 the initial value of the  $E_h$  conditions (Figure 9c,d). However, a recent study has indicated that  
 506 using solely the gaseous  $O_2$  concentration to quantify soil aeration status might be inaccurate for  
 507 some conditions (Ben-Noah et al., 2021). Instead, the authors suggested using the Damkholer  
 508 number, which is the ratio between characteristic diffusion (i.e., oxygen supply) and soil  
 509 respiration times. A small Damkholer number would indicate that the  $O_2$  consumption rate is  
 510 lower than the  $O_2$  supply. Thus, although during summer the oxygen supply rate is relatively  
 511 high compared to winter (**Error! Reference source not found.a,b**), the oxygen consumption  
 512 rate for soil respiration is expected to be substantially higher during summer than during winter  
 513 (Kirschbaum, 1995), as it is reflected by the  $E_h$  observations (Figure 5 and Figure 7). Therefore,  
 514 in parallel to proper treatment of aeration time, optimal wetting time should be further treated.

515

516



517



518 Figure 9: Plot of hourly means of  $E_h$  and gaseous  $O_2$  measurements from the beginning of the drying  
519 stages. The statistics are based on (a,c) 14 cycles during winter (November–April) and (b,d) 19 cycles  
520 during summer (May–October). Note that the gaseous  $O_2$  (a,b) measurements were obtained at 25, 50, 75  
521 and 150 cm depths and the  $E_h$  conditions (c,d) were observed at 25, 50, 75 and 100 cm depths. All  
522 observations were conducted in station 2. The data are separated between summer and winter according  
523 to the trends presented in Figure 5. The green, grey, and yellow areas represent the oxic ( $400\text{mV} <$ ),  
524 suboxic ( $400\text{mV} > E_h > 100\text{mV}$ ), and anoxic ( $E_h < 100\text{mV}$ ) conditions, respectively.

525

#### 526 **4 Summary and Conclusions**

527 Continuous monitoring of  $E_h$ ,  $\theta$ , T, and gaseous  $O_2$  in the vadose zones of SAT infiltration ponds  
528 was carried out for about 600 days. SAT operation was subjected to long and short wetting and  
529 drying cycles and seasonal changes. The datasets enabled the examination of factors that control  
530 the hydrological and geochemical conditions in SAT. Calibrated and validated hydrological  
531 models were applied to investigate the water flow dynamics in the SAT vadose zone.  $E_h$  and  
532 gaseous  $O_2$  observations were averaged to determine seasonal changes and deduce the optimal  
533 length of wetting and drying stages.

534 The examination of the measured  $E_h$  conditions illustrated a noticeable decline to markedly  
535 negative values ( $-450\text{mV} >$ ) during summer and to values between 0 and  $-50\text{ mV}$  during winter.  
536 These  $E_h$  conditions were established following 30 hours of wetting, and no considerable  
537 changes in  $E_h$  conditions were noticeable until the wetting stages ceased. A monthly statistic of  
538 the  $E_h$  measurements illustrated the relationship between the size of the  $E_h$  amplitude and the  
539 seasonal T changes. Furthermore, it is speculated that the limited decrease in  $E_h$  conditions  
540 during winter were due to lower microbial activity. An additional support for this claim is the  
541 reduction in infiltration capabilities following long wetting and drying cycles during winter, as  
542 was indicated by the hydrological models. To define the optimal length of a wetting stage, the  $E_h$   
543 data were averaged and separated between the winter and summer periods. During the summer  
544 period, the optimal time length of a wetting stage, according to  $E_h$  observations, is about 30  
545 hours. Determining the optimal length of a wetting stage during winter is challenging.  
546 Practically, there are no significant differences between  $E_h$  conditions during winter and summer

547 for the first 28 hours of wetting. Thus, the length of a wetting stage during winter should be 30  
548 hours, as in the summer period.

549 The length of a drying stage, following the  $E_h$  observations, should be about 36 hours, regardless  
550 of the initial values of the  $E_h$  conditions and the season. Note that during summer, a longer drying  
551 time is required for the  $E_h$  conditions to attain suboxic conditions. Nevertheless, the gaseous  $O_2$   
552 observations indicated faster aeration rates during summer, which compensate for the very  
553 negative  $E_h$  conditions and allow fast recovery. Following our analysis, we suggest that under the  
554 tested conditions, the length of a drying stage should be 36 hours for winter and summer. Shorter  
555 drying stages would affect SAT efficiency, while applying longer drying stages would reduce the  
556 total hydraulic loads that can be fed to the infiltration basin.

557 Implementing in situ  $E_h$ ,  $\theta$ , T and gaseous  $O_2$  sensors provided continuous high-resolution  
558 observations. These datasets revealed the hydrological and biochemical dynamics in SAT as  
559 imposed by seasonal and operational changes. Analysis of the  $E_h$  and  $O_2$  measurements enabled  
560 the identification of the optimal time lengths of wetting and drying stages. The results indicated  
561 that there is no direct relationship between the length of a wetting stage and a drying stage. Thus,  
562 the operational use of a wetting/drying ratio in SAT management should be reconsidered.

563

## 564 **Acknowledgments**

565 This work was financed within the framework of the German–Israeli Water Technology  
566 Cooperation Program under Project No. WT1601/2689, by the German Federal Ministry of  
567 Education and Research (BMBF), and by the Israel Ministry of Science, Technology and Space  
568 (MOST).

569 **References**

- 570 Amy, G. and Drewes, J.: Soil aquifer treatment (SAT) as a natural and sustainable wastewater  
571 reclamation/reuse technology: Fate of wastewater effluent organic Matter (EfoM) and trace  
572 organic compounds, *Environ. Monit. Assess.*, 129, 19–26, [https://doi.org/10.1007/s10661-006-](https://doi.org/10.1007/s10661-006-9421-4)  
573 9421-4, 2007.
- 574 Arye, G., Tarchitzky, J., and Chen, Y.: Treated wastewater effects on water repellency and soil  
575 hydraulic properties of soil aquifer treatment infiltration basins, *J. Hydrol.*, 397, 136–145,  
576 <https://doi.org/10.1016/j.jhydrol.2010.11.046>, 2011.
- 577 Asano, T. and Cotruvo, J. A.: Groundwater recharge with reclaimed municipal wastewater:  
578 Health and regulatory considerations, *Water Res.*, 38, 1941–1951,  
579 <https://doi.org/10.1016/j.watres.2004.01.023>, 2004.
- 580 Ben-Noah, I., Nitsan, I., Cohen, B., Kaplan, G., and Friedman, S. P.: Soil aeration using air  
581 injection in a citrus orchard with shallow groundwater, *Agric. Water Manag.*, 245, 106664,  
582 <https://doi.org/10.1016/j.agwat.2020.106664>, 2021.
- 583 Berner, R. A.: A new geochemical classification of sedimentary environments, *J. Sediment.*  
584 *Perology*, 51, 359–365, [https://doi.org/https://doi.org/10.1306/212F7C7F-2B24-11D7-](https://doi.org/https://doi.org/10.1306/212F7C7F-2B24-11D7-8648000102C1865D)  
585 8648000102C1865D, 1981.
- 586 Bohrerova, Z., Stralkova, R., Podesvova, J., Bohrer, G., and Pokorny, E.: The relationship  
587 between redox potential and nitrification under different sequences of crop rotations, *Soil Tillage*  
588 *Res.*, 77, 25–33, <https://doi.org/10.1016/j.still.2003.10.006>, 2004.
- 589 Bouwer, H.: Artificial recharge of groundwater: Hydrogeology and engineering, *Hydrogeol. J.*,  
590 10, 121–142, <https://doi.org/10.1007/s10040-001-0182-4>, 2002.
- 591 Brettar, I., Sanchez-Perez, J. M., and Trémolières, M.: Nitrate elimination by denitrification in  
592 hardwood forest soils of the Upper Rhine floodplain - Correlation with redox potential and  
593 organic matter, *Hydrobiologia*, 469, 11–21, <https://doi.org/10.1023/A:1015527611350>, 2002.
- 594 Christensen, T. H., Bjerg, P. L., Banwart, S. A., Jakobsen, R., Heron, G., and Albrechtsen, H. J.:  
595 Characterization of redox conditions in groundwater contaminant plumes, *J. Contam. Hydrol.*,  
596 45, 165–241, [https://doi.org/10.1016/S0169-7722\(00\)00109-1](https://doi.org/10.1016/S0169-7722(00)00109-1), 2000.

597 Cook, F. J. and Knight, J. H.: Oxygen Transport to Plant Roots, *Soil Sci. Soc. Am. J.*, 67, 20–31,  
598 <https://doi.org/10.2136/sssaj2003.2000>, 2003.

599 Díaz-Cruz, M. S. and Barceló, D.: Trace organic chemicals contamination in ground water  
600 recharge, *Chemosphere*, 72, 333–342, <https://doi.org/10.1016/j.chemosphere.2008.02.031>, 2008.

601 Dillon, P.: Future management of aquifer recharge, *Hydrogeol. J.*, 13, 313–316,  
602 <https://doi.org/10.1007/s10040-004-0413-6>, 2005.

603 Doerr, S. H., Shakesby, R. A., and Walsh, R. P. D.: Soil water repellency: Its causes,  
604 characteristics and hydro-geomorphological significance, *Earth Sci. Rev.*, 51, 33–65,  
605 [https://doi.org/10.1016/S0012-8252\(00\)00011-8](https://doi.org/10.1016/S0012-8252(00)00011-8), 2000.

606 Drewes, J. E.: Ground water replenishment with recycled water - Water quality improvements  
607 during managed aquifer recharge, *Ground Water*, 47, 502–505, <https://doi.org/10.1111/j.1745->  
608 [6584.2009.00587\\_5.x](https://doi.org/10.1111/j.1745-6584.2009.00587_5.x), 2009.

609 Dutta, T., Carles-Brangarí, A., Fernández-García, D., Rubol, S., Tirado-Conde, J., and Sanchez-  
610 Vila, X.: Vadose zone oxygen (O<sub>2</sub>) dynamics during drying and wetting cycles: An artificial  
611 recharge laboratory experiment, *J. Hydrol.*, 527, 151–159,  
612 <https://doi.org/10.1016/j.jhydrol.2015.04.048>, 2015.

613 Elkayam, R., Soplinski, A., Gasser, G., Pankratov, I., and Lev, O.: Oxidizer Demand in the  
614 Unsaturated Zone of a Surface-Spreading Soil Aquifer Treatment System, *Vadose Zo. J.*, 14,  
615 [vzj2015.03.0047](https://doi.org/10.2136/vzj2015.03.0047), <https://doi.org/10.2136/vzj2015.03.0047>, 2015.

616 Essandoh, H. M. K., Tizaoui, C., and Mohamed, M. H. A.: Removal of dissolved organic carbon  
617 and nitrogen during simulated soil aquifer treatment, *Water Res.*, 47, 3559–3572,  
618 <https://doi.org/10.1016/j.watres.2013.04.013>, 2013.

619 Fox, P., Aboshanp, W., and Alsamadi, B.: during Soil Aquifer Treatment, 163, 156–163, 2005.

620 Froelich, P. N., Klinkhammer, G. P., Bender, M. L., Luedtke, N. A., Heath, G. R., Cullen, D.,  
621 Dauphin, P., Hammond, D., Hartman, B., and Maynard, V.: Early oxidation of organic matter in  
622 pelagic sediments of the eastern equatorial Atlantic: suboxic diagenesis, *Geochim. Cosmochim.*  
623 *Acta*, 43, 1075–1090, [https://doi.org/10.1016/0016-7037\(79\)90095-4](https://doi.org/10.1016/0016-7037(79)90095-4), 1979.

624 Ganot, Y., Holtzman, R., Weisbrod, N., Nitzan, I., Katz, Y., and Kurtzman, D.: Monitoring and  
625 modeling infiltration-recharge dynamics of managed aquifer recharge with desalinated seawater,  
626 *Hydrol. Earth Syst. Sci.*, 21, 4479–4493, <https://doi.org/10.5194/hess-21-4479-2017>, 2017.

627 Goren, O., Lazar, B., Burg, A., and Gavrieli, I.: Mobilization and retardation of reduced  
628 manganese in sandy aquifers: Column experiments, modeling and implications, *Geochim.*  
629 *Cosmochim. Acta*, 96, 259–271, <https://doi.org/10.1016/j.gca.2012.06.032>, 2012.

630 Goren, O., Burg, A., Gavrieli, I., Negev, I., Guttman, J., Kraitzer, T., Kloppmann, W., and Lazar,  
631 B.: Biogeochemical processes in infiltration basins and their impact on the recharging effluent,  
632 the soil aquifer treatment (SAT) system of the Shafdan plant, Israel, *Appl. Geochemistry*, 48,  
633 58–69, <https://doi.org/10.1016/j.apgeochem.2014.06.017>, 2014.

634 Gorski, G., Fisher, A. T., Beganskas, S., Weir, W. B., Redford, K., Schmidt, C., and Saltikov, C.:  
635 Field and Laboratory Studies Linking Hydrologic, Geochemical, and Microbiological Processes  
636 and Enhanced Denitrification during Infiltration for Managed Recharge, *Environ. Sci. Technol.*,  
637 53, 9491–9501, <https://doi.org/10.1021/acs.est.9b01191>, 2019.

638 Grau-martínez, A., Torrentó, C., Carrey, R., Rodríguez-escalles, P., Domènech, C., Ghiglieri, G.,  
639 Soler, A., and Otero, N.: Feasibility of two low-cost organic substrates for inducing denitri fi  
640 cation in arti fi cial recharge ponds : Batch and fl ow-through experiments, *J. Contam. Hydrol.*,  
641 198, 48–58, <https://doi.org/10.1016/j.jconhyd.2017.01.001>, 2017.

642 Grau-martínez, A., Folch, A., Torrentó, C., Valhondo, C., Barba, C., Domènech, C., Soler, A.,  
643 and Otero, N.: Monitoring induced denitrification during managed aquifer recharge in an  
644 infiltration pond, *J. hydrology*, 561, 123–135, <https://doi.org/10.1016/j.jhydrol.2018.03.044>, 2018.

645 Greskowiak, J., Prommer, H., Massmann, G., and Nützmann, G.: Modeling seasonal redox  
646 dynamics and the corresponding fate of the pharmaceutical residue phenazone during artificial  
647 recharge of groundwater, *Environ. Sci. Technol.*, 40, 6615–6621,  
648 <https://doi.org/10.1021/es052506t>, 2006.

649 Grinshpan, M., Furman, A., Dahlke, H. E., Raveh, E., and Weisbrod, N.: From managed aquifer  
650 recharge to soil aquifer treatment on agricultural soils: Concepts and challenges, *Agric. Water*  
651 *Manag.*, 255, 106991, <https://doi.org/10.1016/j.agwat.2021.106991>, 2021.

652 Grinshpan, M., Turkeltaub, T., Furman, A., Raveh, E., and Weisbrod, N.: On the use of orchards  
653 to support soil aquifer treatment systems, *Agric. Water Manag.*, 260,  
654 <https://doi.org/10.1016/j.agwat.2021.107315>, 2022.

655 Guswa, A. J., Celia, M. A., and Rodriguez-Iturbe, I.: Models of soil moisture dynamics in  
656 ecohydrology: A comparative study, *Water Resour. Res.*, 38, 5-1-5–15,  
657 <https://doi.org/10.1029/2001wr000826>, 2002.

658 Hargreaves, J. A.: Photosynthetic suspended-growth systems in aquaculture, *Aquac. Eng.*, 34,  
659 344–363, <https://doi.org/10.1016/j.aquaeng.2005.08.009>, 2006.

660 Hinchey, E. K. and Schaffner, L. C.: An evaluation of electrode insertion techniques for  
661 measurement of redox potential in estuarine sediments, *Chemosphere*, 59, 703–710,  
662 <https://doi.org/10.1016/j.chemosphere.2004.10.029>, 2005.

663 Ickson-Tal, N., Avraham, O., Sack, J., and Cikurel, H.: Water reuse in Israel – the Dan region  
664 project: evaluation of water quality and reliability of plant’s operation., 3, 231–237, 2003.

665 Inbar, Y.: New standards for treated wastewater reuse in Israel, in: In: Zaidi M, editor.  
666 Wastewater reuse—risk assessment, decision-making and environmental security., Dordrecht,  
667 The Netherlands: Springer; 2007. p. 291–6., 2007.

668 Kfir, O., Tal, A., Gross, A., and Adar, E.: The effect of reservoir operational features on recycled  
669 wastewater quality, *Resour. Conserv. Recycl.*, 68, 76–87,  
670 <https://doi.org/10.1016/j.resconrec.2012.08.002>, 2012.

671 Kirschbaum, M. U. F.: The temperature dependence of soil organic matter decomposition, and  
672 the effect of global warming on soil organic C storage, *Soil Biol. Biochem.*, 27, 753–760,  
673 [https://doi.org/10.1016/0038-0717\(94\)00242-S](https://doi.org/10.1016/0038-0717(94)00242-S), 1995.

674 Lin, C., Greenwald, D., and Banin, A.: Temperature dependence of infiltration rate during large  
675 scale water recharge into soils, *Soil Sci. Soc. Am. J.*, 67, 487–493,  
676 <https://doi.org/10.2136/sssaj2003.4870>, 2003.

677 Lin, C., Eshel, G., Negev, I., and Banin, A.: Long-term accumulation and material balance of  
678 organic matter in the soil of an effluent infiltration basin, *Geoderma*, 148, 35–42,  
679 <https://doi.org/10.1016/j.geoderma.2008.09.017>, 2008.

680 Mächler, L., Peter, S., Brennwald, M. S., and Kipfer, R.: Excess air formation as a mechanism  
681 for delivering oxygen to groundwater, *Water Resour. Res.*, 49, 6847–6856,  
682 <https://doi.org/10.1002/wrcr.20547>, 2013.

683 Massmann, G., Greskowiak, J., Dünnbier, U., Zuehlke, S., Knappe, A., and Pekdeger, A.: The  
684 impact of variable temperatures on the redox conditions and the behaviour of pharmaceutical  
685 residues during artificial recharge, *J. Hydrol.*, 328, 141–156,  
686 <https://doi.org/10.1016/j.jhydrol.2005.12.009>, 2006.

687 McMahon, P. B. and Chapelle, F. H.: Redox processes and water quality of selected principal  
688 aquifer systems, *Ground Water*, 46, 259–271, <https://doi.org/10.1111/j.1745-6584.2007.00385.x>,  
689 2008.

690 Miller, J. H., Ela, W. P., Lansey, K. E., Chipello, P. L., and Arnold, R. G.: Nitrogen  
691 Transformations during Soil–Aquifer Treatment of Wastewater Effluent—Oxygen Effects in  
692 Field Studies, *J. Environ. Eng.*, 132, 1298–1306, [https://doi.org/10.1061/\(asce\)0733-  
693 9372\(2006\)132:10\(1298\)](https://doi.org/10.1061/(asce)0733-9372(2006)132:10(1298)), 2006.

694 Mizrahi, G., Furman, A., and Weisbrod, N.: Infiltration under Confined Air Conditions: Impact  
695 of Inclined Soil Surface, *Vadose Zo. J.*, 15, vzj2016.04.0034,  
696 <https://doi.org/10.2136/vzj2016.04.0034>, 2016.

697 Morrison, C. M., Betancourt, W. Q., Quintanar, D. R., Lopez, G. U., Pepper, I. L., and Gerba, C.  
698 P.: Potential indicators of virus transport and removal during soil aquifer treatment of treated  
699 wastewater effluent, *Water Res.*, 177, 115812, <https://doi.org/10.1016/j.watres.2020.115812>,  
700 2020.

701 Ben Moshe, S., Weisbrod, N., Barquero, F., Sallwey, J., Orgad, O., and Furman, A.: On the role  
702 of operational dynamics in biogeochemical efficiency of a soil aquifer treatment system, *Hydrol.  
703 Earth Syst. Sci.*, 24, 417–426, <https://doi.org/10.5194/hess-24-417-2020>, 2020.

704 Ben Moshe, S., Weisbrod, N., and Furman, A.: Optimization of soil aquifer treatment (SAT)  
705 operation using a reactive transport model, *Vadose Zo. J.*, 1–13,  
706 <https://doi.org/10.1002/vzj2.20095>, 2021.

707 Nadav, I., Arye, G., Tarchitzky, J., and Chen, Y.: Enhanced infiltration regime for treated-

708 wastewater purification in soil aquifer treatment (SAT), *J. Hydrol.*, 420–421, 275–283,  
709 <https://doi.org/10.1016/j.jhydrol.2011.12.013>, 2012a.

710 Nadav, I., Tarchitzky, J., and Chen, Y.: Soil cultivation for enhanced wastewater infiltration in  
711 soil aquifer treatment (SAT), *J. Hydrol.*, 470–471, 75–81,  
712 <https://doi.org/10.1016/j.jhydrol.2012.08.013>, 2012b.

713 Negev, I., Shechter, T., Shtrasler, L., Rozenbach, H., and Livne, A.: The effect of soil tillage  
714 equipment on the recharge capacity of infiltration ponds, 12, 1–11,  
715 <https://doi.org/10.3390/w12020541>, 2020.

716 Nimmo, J. R., Schmidt, K. M., Perkins, K. S., and Stock, J. D.: Rapid Measurement of Field-  
717 Saturated Hydraulic Conductivity for Areal Characterization, *Vadose Zo. J.*, 8, 142–149,  
718 <https://doi.org/10.2136/vzj2007.0159>, 2009.

719 Oren, O., Gavrieli, I., Burg, A., Guttman, J., and Lazar, B.: Manganese mobilization and  
720 enrichment during soil aquifer treatment (SAT) of effluents, the Dan Region Sewage  
721 Reclamation Project (Shafdan), Israel, *Environ. Sci. Technol.*, 41, 766–772,  
722 <https://doi.org/10.1021/es060576+>, 2007.

723 Quanrud, D. M., Arnold, R. G., Wilson, L. G., Gordon, H. J., Graham, D. W., and Amy, G. L.:  
724 Fate of Organics during Column Studies of Soil Aquifer Treatment, *J. Environ. Eng.*, 122, 314–  
725 321, [https://doi.org/10.1061/\(asce\)0733-9372\(1996\)122:4\(314\)](https://doi.org/10.1061/(asce)0733-9372(1996)122:4(314)), 1996.

726 Quanrud, D. M., Hafer, J., Karpiscak, M. M., Zhang, J., Lansey, K. E., and Arnold, R. G.: Fate  
727 of organics during soil-aquifer treatment: Sustainability of removals in the field, *Water Res.*, 37,  
728 3401–3411, [https://doi.org/10.1016/S0043-1354\(02\)00489-X](https://doi.org/10.1016/S0043-1354(02)00489-X), 2003.

729 Reedy, K. R., D’Angelo, E. M., and Harris, W. G.: Biochemistry of wetlands, in: *Handbook of*  
730 *Soil Science*, edited by: Summer, M. E., 89–119, 2000.

731 Rezanezhad, F., Couture, R. M., Kovac, R., O’Connell, D., and Van Cappellen, P.: Water table  
732 fluctuations and soil biogeochemistry: An experimental approach using an automated soil  
733 column system, *J. Hydrol.*, 509, 245–256, <https://doi.org/10.1016/j.jhydrol.2013.11.036>, 2014.

734 Ritter, A. and Muñoz-Carpena, R.: Performance evaluation of hydrological models: Statistical  
735 significance for reducing subjectivity in goodness-of-fit assessments, *J. Hydrol.*, 480, 33–45,



736 <https://doi.org/10.1016/j.jhydrol.2012.12.004>, 2013.

737 Rodríguez-Escales, P., Barba, C., Sanchez-Vila, X., Jacques, D., and Folch, A.: Coupling Flow,  
738 Heat, and Reactive Transport Modeling to Reproduce in Situ Redox Potential Evolution:  
739 Application to an Infiltration Pond, *Environ. Sci. Technol.*, 54, 12092–12101,  
740 <https://doi.org/10.1021/acs.est.0c03056>, 2020.

741 Sallwey, J., Jurado, A., Barquero, F., and Fahl, J.: Enhanced removal of contaminants of  
742 emerging concern through hydraulic adjustments in soil aquifer treatment, 12,  
743 <https://doi.org/10.3390/w12092627>, 2020.

744 Sattar, A. M. A.: Prediction of Organic Micropollutant Removal in Soil Aquifer Treatment  
745 System Using GEP, *J. Hydrol. Eng.*, 21, 04016027, [https://doi.org/10.1061/\(asce\)he.1943-5584.0001372](https://doi.org/10.1061/(asce)he.1943-5584.0001372), 2016.

747 Schmidt, C. M., Fisher, A. T., Racz, A. J., Lockwood, B. S., and Huertos, M. L.: Linking  
748 denitrification and infiltration rates during managed groundwater recharge, *Environ. Sci.*  
749 *Technol.*, 45, 9634–9640, <https://doi.org/10.1021/es2023626>, 2011.

750 Sharma, S. K. and Kennedy, M. D.: Soil aquifer treatment for wastewater treatment and reuse,  
751 *Int. Biodeterior. Biodegrad.*, 119, 671–677, <https://doi.org/10.1016/j.ibiod.2016.09.013>, 2017.

752 Shenker, M., Seitelbach, S., Brand, S., Haim, A., and Litaor, M. I.: Redox reactions and  
753 phosphorus release in re-flooded soils of an altered wetland, *Eur. J. Soil Sci.*, 56, 515–525,  
754 <https://doi.org/10.1111/j.1365-2389.2004.00692.x>, 2005.

755 Silver, M., Knöller, K., Schlögl, J., Kübeck, C., and Schüth, C.: Nitrogen cycling and origin of  
756 ammonium during infiltration of treated wastewater for managed aquifer recharge, *Appl.*  
757 *Geochemistry*, 97, 71–80, <https://doi.org/10.1016/j.apgeochem.2018.08.003>, 2018.

758 Skopp, J., Jawson, M. D., and Doran, J. W.: Steady-State Aerobic Microbial Activity as a  
759 Function of Soil Water Content, *Soil Sci. Soc. Am. J.*, 54, 1619–1625,  
760 <https://doi.org/10.2136/sssaj1990.03615995005400060018x>, 1990.

761 Sopilniak, A., Elkayam, R., and Lev, O.: Nitrification in a soil-aquifer treatment system:  
762 Comparison of potential nitrification and concentration profiles in the vadose zone, *Environ. Sci.*  
763 *Process. Impacts*, 19, 1571–1582, <https://doi.org/10.1039/c7em00402h>, 2017.

764 Sopilniak, A., Elkayam, R., Rossin, A. V., and Lev, O.: Emerging organic pollutants in the  
765 vadose zone of a soil aquifer treatment system: Pore water extraction using positive  
766 displacement, *Chemosphere*, 190, 383–392, <https://doi.org/10.1016/j.chemosphere.2017.10.010>,  
767 2018.

768 Stumm, W., & Morgan, J. J.: *Aquatic chemistry* (3rd ed.), Wiley, 1996.

769 Tsangaratos, P., Kallioras, A., Pizpikis, T., Vasileiou, E., Ilia, I., and Pliakas, F.: Multi-criteria  
770 Decision Support System (DSS) for optimal locations of Soil Aquifer Treatment (SAT) facilities,  
771 *Sci. Total Environ.*, 603–604, 472–486, <https://doi.org/10.1016/j.scitotenv.2017.05.238>, 2017.

772 Tufenkji, N., Redman, J. A., and Elimelech, M.: Interpreting deposition patterns of microbial  
773 particles in laboratory-scale column experiments, *Environ. Sci. Technol.*, 37, 616–623,  
774 <https://doi.org/10.1021/es025871i>, 2003.

775 Wallace, C. D., Sawyer, A. H., and Barnes, R. T.: Spectral analysis of continuous redox data  
776 reveals geochemical dynamics near the stream–aquifer interface, *Hydrol. Process.*, 33, 405–413,  
777 <https://doi.org/10.1002/hyp.13335>, 2019.

778 Wallis, M. G. and Horne, D. J.: Soil water repellency, in: *Advances in Soil Science*, 265–267,  
779 1992.

780

781

782

783

784